INVESTIVATION OF LOW THRUST TO WEIGHT RATIO ROTATIONAL CAPACITY OF ASYMMETRIC MONO-WING CONFIGURATIONS

Derrick Ho*, Dr KC Wong*
School of Aerospace, Mechanical and Mechatronic Engineering, The University of Sydney
Aeronautical Engineering Building J11,
The University of Sydney, NSW, 2006, Australia
derrick.ho@sydney.edu.au

Keywords: *bio-inspiried, monocopter, asymmetric, UAV*

Abstract

This paper explores the potential of bio-inspired bi-mode UAV concepts by investigating low thrust to weight ratio rotational capacity of asymmetric mono-wing configurations using a single lifting surface. Adapted blade element theory for low Reynolds number with tip losses is employed to estimate rotational capacity of lifting surface specimens which are empirically validated to draw recommendations to aid future design.

1 Introduction

Modern urban and hostile operational requirements desire a platform with broad flight spectrum, high manoeuvrability and vertical takeoff and landing (VTOL) including hover which exceeds the capability of many existing Unmanned Aerial Vehicles(UAVs). Ongoing technological advancements allows alternative concepts which were once deemed unfeasible to be re-explored such as bi-mode UAV concepts [1] which can interchange configurations to broaden the flight spectrum and enhance overall mission capability. Increasing understanding and growing interest in biological flyers have seen the spawning of bio-inspired platforms to mimic nature's superiority and efficiency in flight to address new mission demands. One particular example is the single-bladed monocopter inspired by the falling Samara seed [2] as a highly efficient asymmetric all-rotating hovering platform. Another example is the flying wing systems which imitate the simplicity of the symmetric fixed-wing tailless flying of birds. Emerging from the investigations into nature's superior flyers, a fusion of the monocopter and flying wing characteristics presents a novel bi-mode bio-inspired UAV concept where low thrust to weight hover [1] can be achieved whilst offering high cruise efficiency.

The proposed concept utilises a common lifting surface for both rotational and non-rotational flight. Fig.1(a) shows one possible evolution which adapts a monocopter for conventional fixed-wing forward flight. Conversely, Fig.1(b) shows the conventional fixed-wing forward flight evolving into a potential rotational platform.

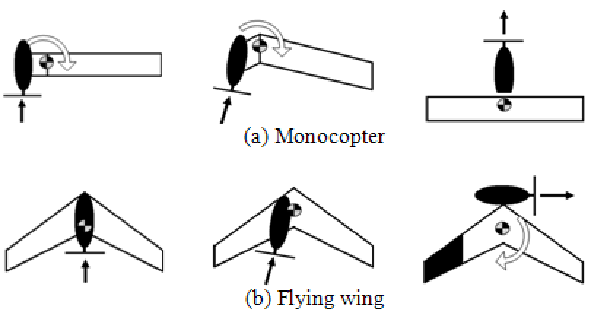

Fig.1: Potential evolution paths from rotational to non-rotational flight of a platform capable of interchangeable configurations.

While the asymmetry of the monocopter and symmetry of the flying wing mono-wing configurations are understood separately, relationships amongst the basic parameters for interchanging between the two using a common lifting surface currently remains unexplored. The effect of the driving parameters for rotational flight [3] is explored to assist in drawing correlations with the flying wing counterpart.

2.1 Theoretical Model Prediction

Adapted blade element theory [4] for low Reynolds number with tip losses is employed to estimate rotational capacity of a range of lifting surface specimens. Discretising the lifting surface into elements allows local flow analysis that is summated to yield the overall result.

The local velocity experienced by the lifting surface is influenced by the axial and radial components as shown below in Fig.2:

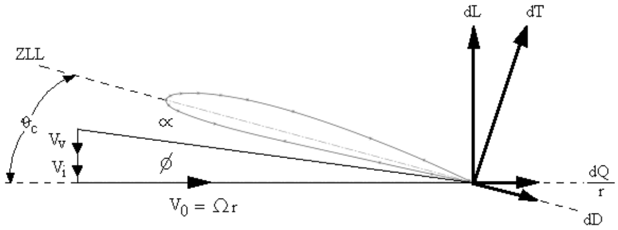

Fig.2: Aerodynamic angles

The induced velocity v_i is given as below which is solved using quadratic formulation:

Induced Velocity expression:

$$v_i^2\left(\frac{1}{\Omega R}\right)^2 + v_i\left(\frac{v_v}{\Omega R} + \frac{a\sigma}{8}\right) - \left[\frac{a\sigma}{8}\left(\theta_c x - \left(\frac{v_v}{\Omega R}\right)\right)\right] = 0$$

Upon solving:

$ax^2 + bx + c = 0 \quad \Rightarrow \quad x = \frac{-b \pm \sqrt{b^2 - 4ac)}}{2a}$ yields:

Quadratic induced velocity expression:

$$\frac{v_i}{\Omega R}\left[\frac{1}{2}\left(\frac{v_v}{\Omega R}\right) + \frac{a\sigma}{16}\right]\left[-1\left\{1 + \frac{a\sigma}{2}\left[\left(\theta_c x - \frac{v_v}{\Omega R}\right)\left(\frac{v_i}{\Omega R} + \frac{a\sigma}{8}\right)\right]^{-2}\right\}^{-\frac{1}{2}}\right]$$

Similarly an alternative expression [4] for induced velocity is also employed:

Stepniewski induced velocity expression:

$$V_i = V_t\left[-\frac{a\sigma}{16} + \sqrt{\left(\frac{a\sigma}{16}\right)^2 + \frac{a\sigma\bar{r}}{8}(\theta_o - \theta_{tot}\bar{r})}\right]$$

The aerodynamic angles can be evaluated as:

θ_c	geometric pitch	$= \theta_{collective} + \theta_{twist}$
ϕ	pitch decrement due to induced flow(s)	$= \frac{V_i + V_v}{V_r}$
α	angle of attack	$= \theta_c - \phi$

Summation of discrete elements from each blade element is summarised by:

$$Thrust = T = \sum dT$$

$$Torque = Q = \sum \frac{dQ}{r} r$$

2.2 Empirical Estimations

Test apparatus with pitch, coning and rotational freedom is used to empirically validate the theoretical predictions with schematic shown below in Fig.3(a) and the test apparatus shown in Fig.3(b). A tip thrusters offset from the pivot generates rotational motion for VTOL and hover applications.

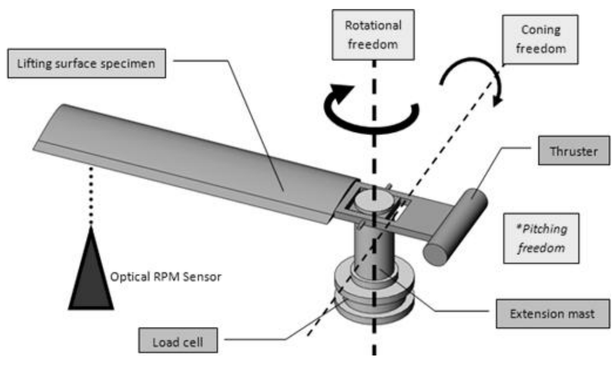

Fig.3(a): Schematic of apparatus.

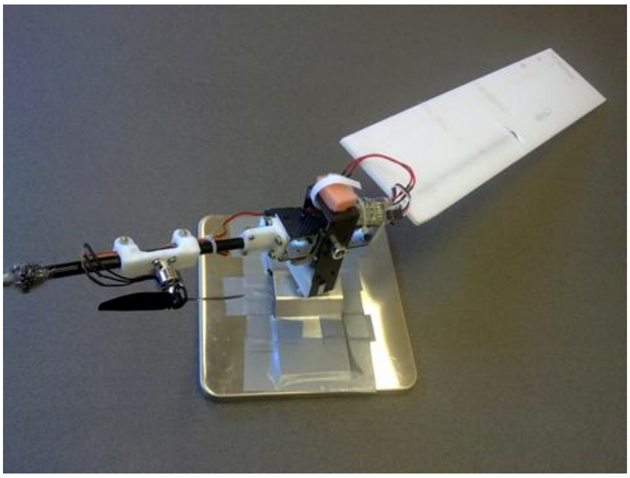

Fig.3(b): Test apparatus

The apparatus rests upon a load cell which enables lift(thrust) measurements within ±1g and the coning angle and pitch angles measured by a digital protractor accurate to ±0.1°. Rotational rate is measured with an optical tachometer accurate to ±1RPM between 0-999RPM.

3.0 Result Validation and Analysis

The test specimen specification involves the following parameters of a single mono-wing offset with a tip thruster:

Span	0.45m
Aspect ratio(AR)	4.5 and 6.0
Motor Span-wise position	0.45%
Aerofoil section	Flat plate

Table.1: Lifting surface specimen specifications

3.1 Thrust and Rotational

The theoretical prediction and experimental results for thrust versus rotation are shown in Fig.4(a) for AR=4.5 and Fig.4(b) for AR=6.0. It can be seen in Fig.4(a) has close correlation for the range of $\alpha=5°$ to $\alpha=25°$. Fig.4(b) show close correlation up to an angle of attack of $\alpha=20°$ where separation and stall occurs between $\alpha=15°$ and $\alpha=20°$ reflecting the theoretical predictions are accurate up to the point of flow separation.

Extrapolation of the thrust and torque distribution over the lifting surface is shown in Fig.5(a). Majority of lift occurs at the tips where radial velocity and Reynolds number is highest suggesting concentrating lifting surface area at the tip is effective for monocopter configurations [3] exemplified in Fig.5(b).

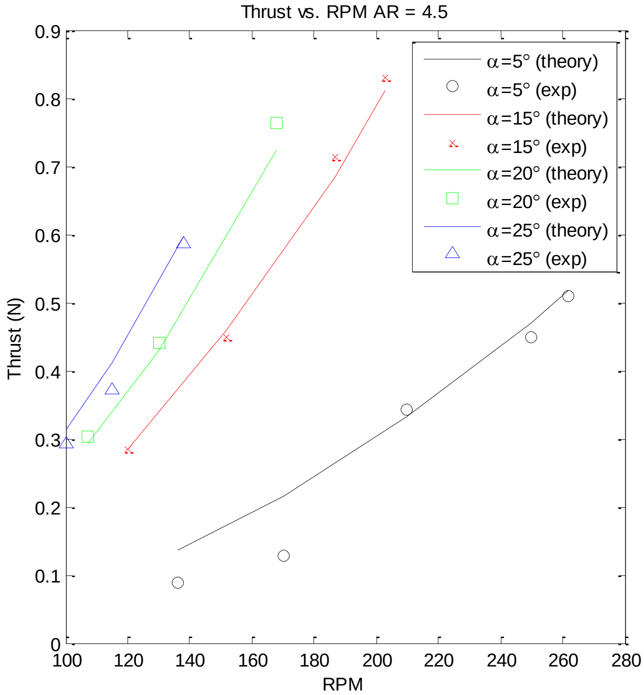

Fig.4(a): Aspect ratio = 4.5.

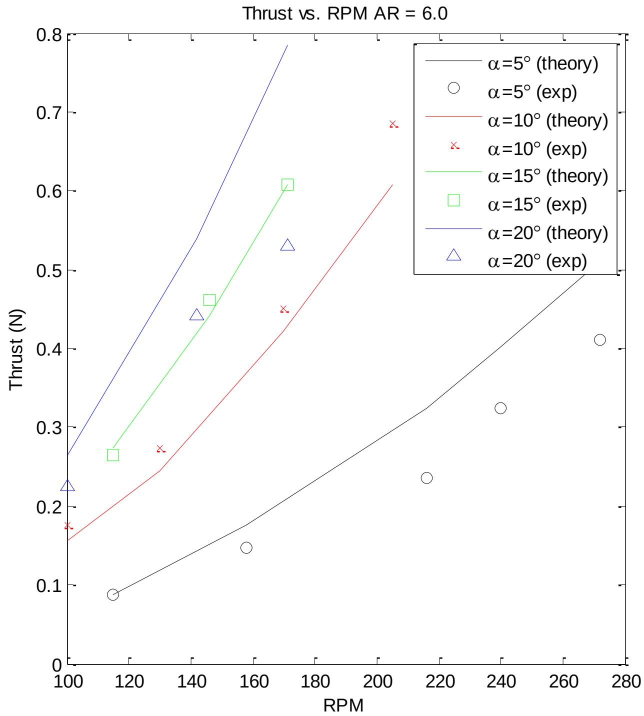

Fig.4(a): Aspect ratio = 6.0.

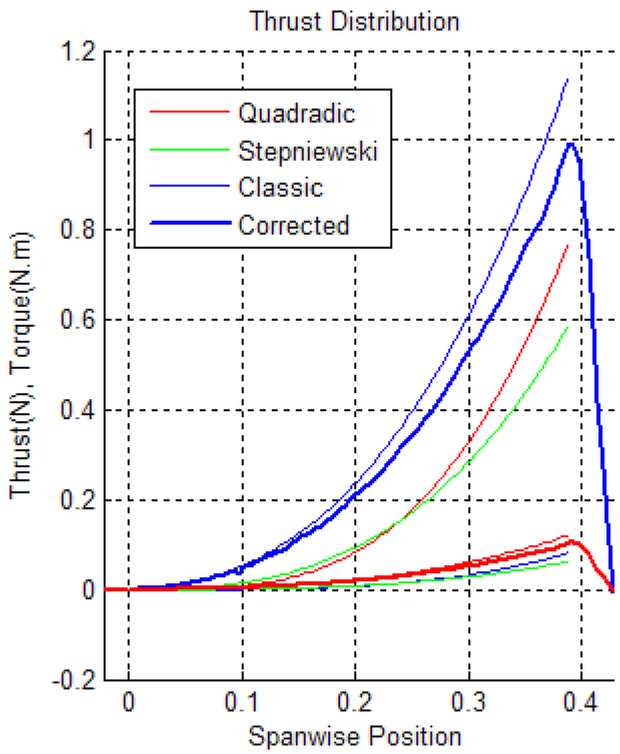

Fig.5(a): Thrust distribution over lifting surface for AR = 4.5 specimen.

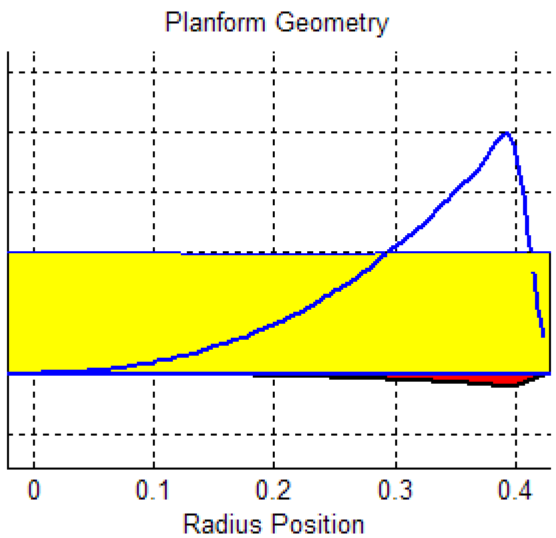

Fig.5(b): Figurative illustration of lift and drag over the lifting surface specimen

Induced velocity profile is shown in Fig.6 along with Reynolds number variation for the AR=4.5 specimen which shows small monocopter application reside in the very low Reynolds number operation.

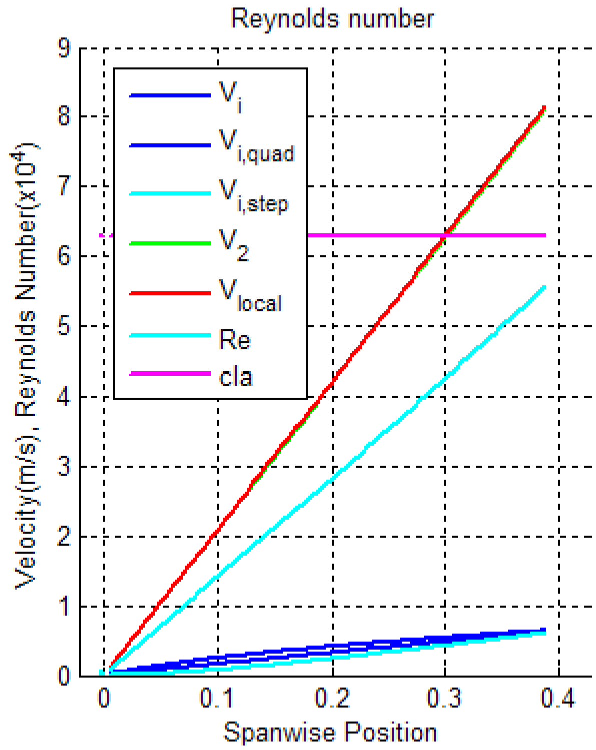

Fig.6: Reynolds number and velocity profile predictions over the lifting surface.

The main aerodynamic angles can be seen in Fig.7 where higher lift to drag ratio occurs inboard of the lifting surface along with the local α after induced flow corrections.

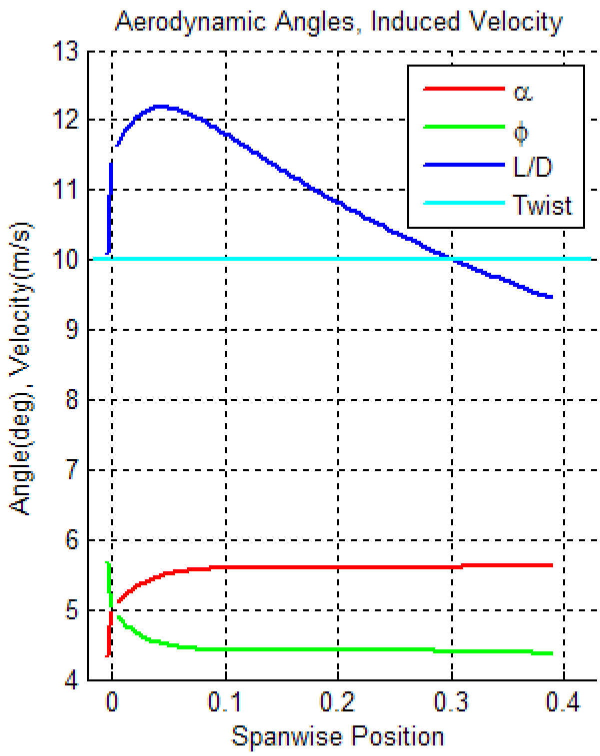

Fig.7: Aerodynamic angles.

The coning angle in Fig.8 for a set motor incidence sees the coning angle increase with higher AR due to the shift in center of pressure of the lifting specimen relative to the point of rotation.

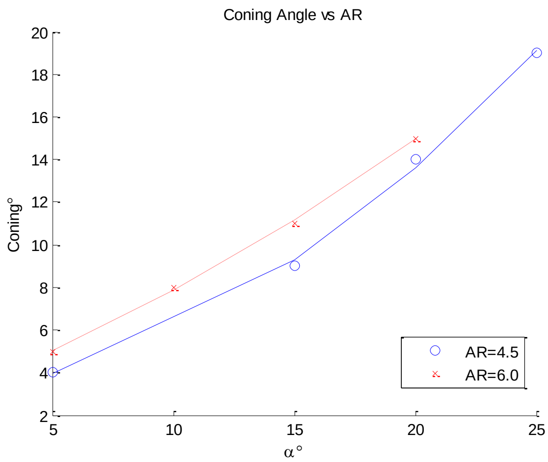

Fig.8. Coning angle for AR=4.5 and AR=6.0.

To reduce coning angle, an offset thruster incidence is needed to balance the lifting force; it is a corollary that a particular motor incidence would also dictate the natural coning angle.

3 Conclusions and Recommendations

The analysis of the basic parameters allows further consideration to monocopter design and ultimately greater understanding towards asymmetric rotational and asymmetric conventional flight. Based on observations and trends from the preliminary data, conclusions and recommendations are drawn with insight directed to monocopter and flying wing design which are listed as follows:

- Blade element theory adapted to low Reynolds number with tip loss corrections allow accurate modelling and prediction of small mono-wing lifting surfaces which can be used to aid future analysis

- If span is kept constant (0.45m in this case study) and if AR is increased, rotational rate is increased as less drag is generated. For higher AR to produce the same lift as lower AR at the same rotational rate, α must be increased accordingly which is similar to changing AR in conventional flying wing design.

- The lift distribution and majority of contributing lift resides at the tips of the monocopter whilst the majority of lift would occur on the inboard for flying wings which poses an optimisation challenge.

- Monocopters would benefit from increased thrust line incidence to reduce coning angle to aid moment balance. Reduced coning angle virtually increases span and lifting area. Large thrust line offsets in conventional flying wing would require larger control surface deflections to balance the moment which increases trim drag.

4 Acknowledgements

Author would like to thank the support of many researchers and in particular those associated with the UAV Lab at The University of Sydney.

References

[1] Ho, D, “Low thrust to weight ratio manoeuvre of a bio-inspired bi-mode uav”, School of Aerospace, Mechanical and Mechatronic Engineering, The University of Sydney, 2011

[2] Jamerson, S, et al, “Design of the samarai monowing rotorcraft nano air vehicle”, Lockheed Martin Advanced Technology Laboratories”, n.d.

[3] Ulrich, E.R., Pines, DJ, “Planform geometric variation, and its effect on the autorotation efficiency of a mechanical samara”, Department of Aerospace Engineering, University of Maryland, 2008

[4] Stepniewski W.Z., Keys C.N., "Rotary-wing aerodynamics", 1981

Copyright Statement